A Hybrid SNMP–STP-Based Framework for Topology Discovery and Energy Optimization in Heterogeneous Power Information Networks

Eerdun[1,*], Jianzhong Yang[2], Dongxing Liu[3], Ke Shi[1], Jing Li[1]
[1]Digital Application Laboratory, Digital Research Branch Company of Inner Mongolia Power (Group) Co., LTD
Hohhot 010000, China
[2]Inner Mongolia Power (Group) Co., LTD
Hohhot 010000, China
[3]Inner Mongolia Power Group Mengdian Information & Telecommunication Co., LTD
Hohhot 010000, China
E-mail: fhbdggf38656@163.com, yangjianzhong0325@163.com, liudongxing0325@163.com, shike0325@163.com, lijing0325@163.com
*Corresponding author

Keywords: Digital power systems, network topology, energy efficiency optimization, optimization strategies

Received: September 28, 2025

The rapid development of new power systems and the pursuit of "dual-carbon" goals present power information systems with new challenges: diverse terminal access, dynamic network topologies, and complex load distributions. Traditional topology management and energy efficiency strategies fall short of the requirements for managing heterogeneous networks, VLAN isolation, and dynamic access efficiently. This study proposes an adaptive weight SNMP-STP hybrid topology discovery and energy-efficiency optimization framework that integrates an improved Simple Network Management Protocol (SNMP) with an enhanced Spanning Tree Protocol (STP). The algorithm first performs SNMP scanning to identify device vendor types, response delays, and MIB completeness, which are used to calculate initial weights. It then concurrently collects SNMP-layer routing and port status information along with STP link connectivity data, and constructs a topology matrix based on weight fusion. During operation, weights are dynamically updated, giving priority to high-weight vendor parsing results while incorporating MIB verification and STP status compensation to ensure topology integrity. In parallel, a correlation model between topology parameters and energy consumption is established, enabling coordinated topology recognition and energy-efficiency optimization. Experiments were conducted in a multi-vendor heterogeneous network environment, including 15 routers, 32 switches, and 50 servers. Results demonstrate that the framework achieves 96% topology identification accuracy, a link misjudgment rate below 4%, and a topology update latency of only 150 ms, significantly outperforming traditional methods. The energy-efficiency optimization strategy, based on redundant link sleep and dynamic load balancing, reduced overall system energy consumption by over 30%, with switch energy savings reaching 44.4%. These findings indicate that integrating topology information with energy-efficiency modeling not only enhances system performance and resource utilization but also provides a feasible approach for building low-carbon, efficient, and secure next-generation power information systems, highlighting both theoretical and engineering significance.

Povzetek: Študija predstavlja sistem za učinkovitejše upravljanje omrežne topologije in porabe energije v elektroenergetskih informacijskih sistemih, ki izboljšuje zanesljivost delovanja ter zmanjšuje porabo energije.

1 Introduction

With the advancement of the “dual-carbon” strategy and the rapid development of new power systems, the power industry is accelerating its shift toward digitalization and intelligence. The large-scale integration of intelligent substations, distributed energy terminals, and electricity information collection systems has sharply increased the number of nodes in power information networks and the frequency of topology changes [1]. As the “vascular architecture” of these systems, network topology management directly affects operational continuity and cost-effectiveness [2]. Currently, the reliability requirements for key services such as scheduling automation have increased. In power information systems, “critical services” encompass three core business types, all of which must comply with stringent Service Level Agreements (SLAs): (1) Scheduling automation service: Responsible for real-time issuance of grid load adjustments and fault isolation commands. The SLA specifies a command transmission latency ≤ 500 ms and annual availability ≥ 99.99%. Delays in topology updates

can cause command issuance lag, increasing the risk of grid load imbalance. (2) Distributed photovoltaic (PV) monitoring service: Requires real-time acquisition of PV inverter output voltage and current data with a sampling period of 10–30 s. The SLA mandates that data transmission interruptions ≤ 300 ms per event and data integrity ≥ 99.9%. Untimely identification of topology changes can lead to deviations in PV output forecasting, reducing the grid's power absorption capability. (4) Electric vehicle (EV) charging control service: Handles the interaction of charging power regulation and overload protection commands. The SLA requires a control command response latency ≤ 400 ms and a service interruption rate ≤ 0.1%. Delayed topology updates may disrupt communication between charging terminals and the dispatch center, increasing the probability of EV charging equipment overload failures [3]. Network equipment already accounts for up to 35% of total energy use, with nearly one-fifth of this consumption caused by flaws in topology design [4]. This emphasis on topology accuracy over energy efficiency conflicts with the industry's low-carbon transition goals. Existing topology discovery technologies face two key bottlenecks. First, the widely used SNMP protocol struggles with compatibility in multi-vendor environments. Because vendors define MIB libraries inconsistently, some proprietary OIDs cannot be parsed by standard algorithms, lowering topology recognition accuracy [5]. Second, most physical-layer topology identification methods overlook energy considerations. Algorithms such as STP suppress loops but fail to account for port power or link load, leaving many redundant links operating in "high-energy, low-utilization" states [6]. NTDS systems have improved recognition efficiency through clustering but ignore energy efficiency [7]. Static shutdown of redundant links can reduce energy use but disregards the risks posed by dynamic topology changes [8]. Energy-aware routing offers adaptability but falls short of meeting the strict security partitioning requirements of power systems [9].

Based on the aforementioned research background and existing bottlenecks, this study addresses the following research questions: (1) In multi-vendor heterogeneous power information networks, can a topology-aware energy-efficiency co-optimization strategy significantly outperform device-level energy-efficiency approaches (e.g., dynamic frequency modulation) while simultaneously satisfying the SLAs of critical services? (2) Can an improved SNMP and enhanced STP hybrid topology discovery algorithm achieves higher topology identification accuracy, lower link misjudgment rates, and reduced topology update latency in highly heterogeneous networks with complex VLAN isolation scenarios? (3) Can a topology–energy consumption correlation model enables unified modeling of topology identification and energy-efficiency optimization, thereby providing effective support for dynamic energy-efficiency strategies? To address these questions, the core research objectives are defined as follows: Design an SNMP–STP hybrid topology discovery algorithm with adaptive weighting to resolve MIB conflicts among multi-vendor devices and enhance both the accuracy and dynamic responsiveness of topology identification in heterogeneous environments. (1) Construct a topology–energy correlation model to achieve joint perception of topology states and energy-consumption characteristics, overcoming the limitations of traditional approaches that separate topology discovery from energy optimization. (2) Propose a topology-feature-based dynamic energy-efficiency optimization strategy that significantly reduces overall system energy consumption while ensuring compliance with SLAs for critical services. To validate the feasibility of these objectives, the following hypotheses are proposed: Hypothesis 1: In heterogeneous environments where the proportion of vendor-specific devices is ≤ 80%, the adaptive-weight SNMP–STP hybrid algorithm achieves a topology identification accuracy ≥ 95%, a link misjudgment rate < 5%, and topology update latency ≤ 200 ms, significantly outperforming traditional SNMP (accuracy ≤ 85%) and single STP algorithms (misjudgment rate ≥ 18%). Hypothesis 2: The topology–energy correlation-based co-optimization strategy can reduce overall system energy consumption by over 15% compared with strategies relying solely on device-level dynamic frequency modulation (DFM), with switch energy-saving rates ≥ 40%.

To address these challenges, this study proposes a comprehensive topology analysis framework for digital power information systems. It introduces a hybrid topology discovery algorithm and an energy efficiency optimization strategy driven by topology characteristics. The main contributions are: (1) integrating topology discovery and energy management by mapping link characteristics (e.g., bandwidth, latency) to energy consumption parameters (e.g., port power, load rate), enabling joint awareness of topology and energy states; (2) developing an adaptive-weight SNMP–STP hybrid algorithm that dynamically adjusts the parsing weights of vendor-specific protocols to improve recognition accuracy in multi-vendor environments; and (3) proposing a topology-feature-based dynamic energy-efficiency optimization strategy. This strategy leverages the spatiotemporal characteristics of power system services to reduce network energy consumption. It achieves this through methods such as intelligently putting redundant links to sleep and performing load-balancing migrations. This framework supports efficient operation and maintenance of power information systems and provides theoretical and practical guidance for the low-carbon operation of next-generation power networks.

2 Related work

The evolution of network topology discovery technologies in power information systems has followed three stages, each shaped by the sector's specific requirements. The first relied on ICMP-based probing. Onyema et al. applied Ping and Traceroute commands for node identification. Although simple, these methods cannot penetrate security isolation devices, limiting cross-region recognition and rendering them unsuitable for critical scenarios like dispatch automation [10]. The second stage centered on

SNMP. Del et al. reported that, while systems such as HP OpenView supported SNMP extensions, their real-time performance and adaptability were insufficient for China's partitioned power system architectures [11]. The third stage introduced machine learning. Monkam et al. developed the NTDS system, which applied K-means clustering to device response features, significantly improving node recognition speed [12]. However, these methods still focus on connectivity and overlook energy parameters such as port power and link load, limiting their usefulness for energy optimization in low-carbon systems.

Recent studies have explored the application of adaptive control theory to enhance system responsiveness under uncertain and dynamic conditions. Fuzzy control methods offer advantages in handling measurement noise, incomplete topology information, or load fluctuations—for example, by performing online port power adjustments and link sleep decisions based on empirical rules. However, their limitation lies in focusing primarily on local device states, lacking a global perception of the entire network topology. Yuan et al. proposed that neural adaptive control leveraged the function approximation capability of neural networks to perform online identification of system dynamics and achieve adaptive power scheduling, providing robustness against load variations and topology changes [13]. Rospawan et al. proposed adaptive backstepping control, which designs control laws layer by layer in single-input single-output or multivariable nonlinear systems to ensure stability and tracking performance [14], offering a theoretical reference for energy-efficient scheduling of distributed nodes. Other approaches, such as the application of adaptive fuzzy control in fixed-time synchronization of fractional-order chaotic systems [15], output-feedback projection-based lag synchronization control for uncertain nonlinear chaotic systems [16], and nonlinear optimal control for gas compressor drive systems [17], further demonstrate the potential of adaptive control to handle uncertainty, nonlinearity, and multivariable coupling in complex dynamic systems.

Research on energy efficiency optimization also suffers from "local breakthroughs but overall gaps." Logeshwaran et al. focused on servers and proposed dynamic frequency scaling based on CPU utilization to reduce energy consumption, but they did not consider the overall impact of network topology [18]. Guan et al. integrated topology into energy efficiency by proposing the static shutdown of redundant links. While effective in experiments, it lacked dynamic association model, which limited its real-world applicability [19].

In summary, existing research either prioritizes topology recognition accuracy while neglecting energy-related parameters or focuses on device-level energy management without structural optimization at the network level. No comprehensive approach currently supports both dynamic topology awareness and collaborative energy optimization. To address this issue, a topology discovery mechanism was proposed that combined an improved SNMP protocol with an enhanced Spanning Tree Protocol (STP). By mapping link characteristics to energy consumption parameters, joint modeling of topology and energy states was achieved. Based on this foundation, a dynamic energy optimization strategy was designed. Compared to existing methods, this approach improves adaptability in multi-vendor heterogeneous environments, meets security isolation requirements, and enhances energy awareness, providing theoretical and practical guidance for green, efficient next-generation power information systems. The comparison of related studies has been summarized in Table 1.

Table 1: Summary comparison of related studies

Researcher & Year	**Main Method**	**Application Domain**	**Key Findings**	**Limitations**
Onyema et al., [10], 2022	ICMP-based probing	Power communication networks	Node identification rate ≈ 78%	Cannot penetrate isolation devices; limited cross-region identification capability
Del et al., [11], 2024	SNMP-based topology analysis	Power dispatch systems	Topology identification accuracy 85%	Poor multi-vendor compatibility; relatively high latency
Monkam et al., [12], 2024	K-means clustering for NTDS systems	Smart distribution networks	Node identification speed improved by 25%	Energy-efficiency parameters not considered
Yuan et al., [13], 2014	Neural adaptive control	Nonlinear control systems	Enhanced dynamic robustness	Slow parameter convergence
Rospawan et al., [14], 2024	Adaptive backstepping control	Multivariable nonlinear systems	Achieved stable synchronization control	High real-time requirements
Logeshwaran et al., [18], 2024	Dynamic frequency modulation (DFM)	Server energy optimization	Reduced energy consumption by ~15%	Not combined with topology information

Guan et al., [19], 2023	Static redundant link shutdown	Power communication systems	Reduced energy consumption by ~22%	Lacks dynamic response mechanism

3 Digital power information system topology framework design

3.1 Topology management

Topology management aims to reveal the connectivity among internal network devices, including routers, switches, servers, and hosts [20]. This module uses various topology discovery algorithms to automatically scan the network, collecting detailed information from both network and physical layers. It identifies device types and accurately maps backbone links, redundant channels, and backup paths, providing essential support for network monitoring and optimal resource allocation. An example of the administrator use case in the user management module is shown in Figure 1.

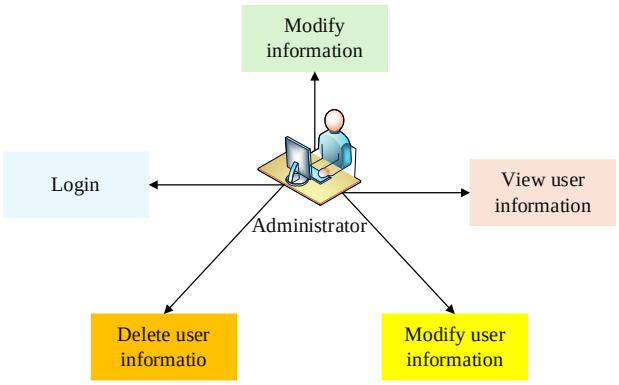

Figure 1: Administrator use cases of the user management module

Administrators are granted the following permissions: configure initial parameters, execute topology data collection tasks, view network- and physical-layer topology diagrams, adjust device display names, query detailed device attributes, monitor performance metrics, and interactively zoom, drag, and export topology diagrams [21]. The specific use case relationships of topology management functions are shown in Figure 2.

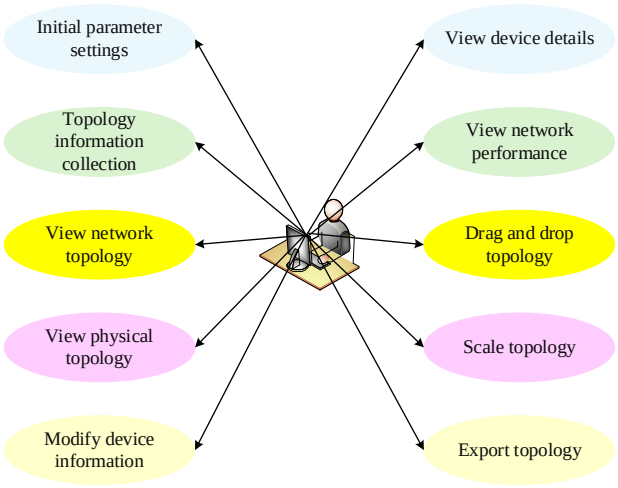

Figure 2: Topology management module diagram

Initial configuration covers key network parameters, including router IP address, SNMP version, read–write authentication passwords, and communication ports. Topology information collection relies on discovery algorithms to automatically scan all devices across the network. Data collection devices can traverse power system security isolation mechanisms, with collected data aggregated and uploaded to the information management domain for centralized processing by the topology discovery host.

In topology visualization, the system analyzes, classifies, and stores collected data to present a real-time network structure. The device information query module displays essential attributes such as IP and MAC addresses, aliases, categories, hierarchy levels, manufacturers, and network status, while indicating SNMP support. Network performance monitoring provides live tracking of key indicators, including port traffic, packet loss, and error rates.

Users can edit device identifiers by renaming aliases and adding notes. Interactive topology graph functions allow node dragging to optimize layout and support zooming operations. The system also enables exporting topology diagrams in specified formats for local storage, facilitating later analysis and archiving. Figure 3 outlines the overall system requirements.

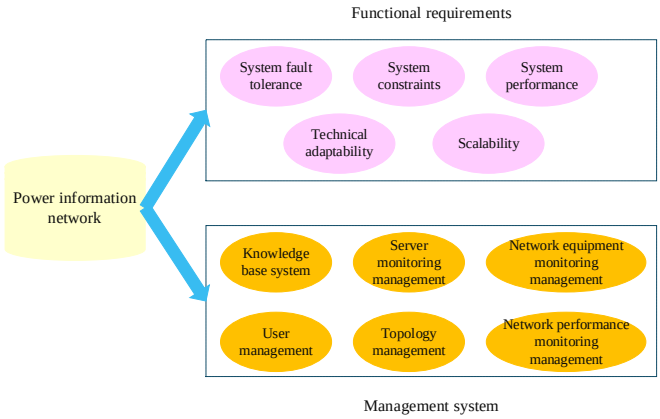

Figure 3: Overall system requirements

In designing the topology management module, the system not only supports topology collection, visualization, and device management but also provides standardized interfaces and data structures for interaction with external adaptive controllers, such as fuzzy controllers or neural adaptive control units. The module delivers real-time inputs as temporally aggregated and semantically annotated state vectors. These include the topology relationship matrix of nodes and links, per-port temporal power spectra, link load distribution curves, VLAN mappings, inter-domain routing tables, and event-driven port status change streams. These vectors can be directly used as fact sets for fuzzy rule-based reasoning or as training/online-update samples for neural adaptive models. This design allows external controllers to consider both topology semantics and energy consumption characteristics when performing energy-efficiency scheduling or redundant-link sleep decisions. In addition, the module provides a policy execution channel to issue fine-grained actions generated by the controllers, such as port sleep commands, link priority adjustments, and load migration instructions. It also collects post-execution energy and topology feedback, supporting closed-loop adaptive learning and maintaining system stability.

The adaptive-weight hybrid SNMP–STP topology discovery algorithm identifies topology concurrently at both logical and physical layers. It fuses and optimizes information across devices from different vendors using a weight-adjustment mechanism, achieving high-precision topology discovery while enabling energy-efficiency scheduling. In heterogeneous environments, adaptive weights correct for differences in device identification confidence. During energy-optimization, port load thresholds trigger dynamic sleep of redundant links, balancing topology accuracy with energy savings. The algorithm proceeds through the following steps:

1) Device identification and weight initialization: The system scans network devices via SNMP to identify vendor type, response time, and MIB completeness for each node. Initial vendor weights are calculated based on device response latency and OID completeness. These weights are normalized to ensure comparability across vendors during topology computation.
2) Topology information collection and fusion: SNMP routing tables and port status tables, along with STP link connectivity information, are collected in parallel. Timestamp matching ensures data synchronization. Vendor weights are applied to perform weighted fusion of SNMP and STP data, producing an initial topology matrix.
3) Multi-vendor MIB conflict detection and resolution: Conflicts in MIB entries describing the same link across different devices are detected. The result from the highest-weight vendor is prioritized when conflicts exist. If confidence levels are close, MIB hash consistency checks validate the OID semantic structures. Remaining uncertain links are compensated using STP port status information to ensure topology completeness.
4) Adaptive weight dynamic update: The algorithm continuously monitors device performance during operation. Vendor weights are periodically updated and immediately incorporated into subsequent link confidence calculations and conflict resolution.
5) Link confidence calculation and verification: Link confidence, Conf(e), is computed by integrating SNMP and STP data. Links with Conf(e)$\geq\theta_{conf}$ are confirmed as valid connections. Others are temporarily marked as candidates and periodically rechecked to avoid misclassification due to short-term network fluctuations.
6) Port sleep triggering and energy-efficiency optimization: Port load rates ρ(p) and historical utilization changes are continuously monitored. When $\rho(p) < \theta_{sleep}$ and the load change rate h(p) < δ (e.g., θ_{sleep} = 20%, δ = 0.05), the port sleep mechanism is triggered. Sleeping ports are automatically removed from the STP-generated tree. Network connectivity is dynamically maintained based on service priority. Sleep states and energy savings are recorded in the energy-optimization table for further evaluation and policy adjustment.
7) Topology graph construction and output: The algorithm outputs a comprehensive topology graph $G(V, E)$ that integrates both logical and physical links. Each link is annotated with confidence and energy status, providing essential data support for subsequent energy-efficiency optimization and scheduling tasks.

When the topology management module implements topology discovery using the hybrid SNMP–STP algorithm, it incorporates a multi-level security enhancement mechanism to address SNMPv3 protocol security risks and access control requirements, thereby ensuring the safety of critical power infrastructure networks. At the protocol configuration level, the module abandons the weak authentication modes of traditional SNMPv1/v2c and adopts the SNMPv3 User-based Security Model (USM). All active query messages, such as GetRequest requests for MIB objects like ipAddrTable and ipRouteTable, are protected with both authentication and encryption. SHA-256 is used for authentication to guarantee message integrity and verify the sender's identity, while AES-256 is used for encryption to prevent eavesdropping or tampering of MIB data during transmission. Query frequency and scope are also strictly controlled. For critical devices such as core routers and switches, the query interval is set to 30 seconds. Only MIB subtrees directly related to topology discovery are queried. Sensitive MIB nodes, such as device configurations and security keys, are blocked using MIB views to prevent information leakage. At the access control level, a role-based access control (RBAC) mechanism with fine-grained permissions is employed. Topology discovery hosts are granted read-only privileges and are bound to specific physical ports and IP addresses, preventing unauthorized devices from masquerading as discovery hosts. Two administrative roles are defined: the Operations Administrator, who can view topology data

only, and the Security Administrator, who can configure SNMP security parameters. All privileged operations require two-factor authentication and generate audit logs, satisfying the power system's requirements for operational traceability and security compliance.

3.2 Network topology structural parameters

Networks are often represented as graphs. Based on graph theory, a graph is defined as an ordered pair G(V, E), where V is the set of nodes and E is the set of edges. Each edge corresponds to a physical link connecting two nodes. Network topology is generally described by the microscopic distribution or statistical averages of a specific graph G(V, E). Understanding structural properties is crucial for exploring dynamic evolution mechanisms and enhancing network robustness [22, 23].

(1) Network Diameter, Density, and Average Path Length

For any pair of nodes (*i, j*), the shortest path d_{ij} is defined as the minimum number of edges connecting them. The network diameter *D* is the largest shortest path among all node pairs:

$$D = \max_{i,j \in V} d_{ij} \tag{1}$$

The average shortest path length *L* is calculated by averaging d_{ij} over all node pairs:

$$L = \frac{2}{n(n-1)} \sum_{i \neq j} d_{ij} \tag{2}$$

where *n* is the total number of nodes. *L* is a key indicator of the network's small-world property.

Network density *d(G)* is the ratio of existing edges to the maximum possible edges, reflecting network connectivity:

$$d(G) = \frac{2m}{n(n-1)} \tag{3}$$

where *m* is the total number of edges.

(2) Node Degree and Its Distribution

The degree k_i of a node *i* represents the number of nodes directly connected to it. The average degree ⟨k⟩, given by ⟨k⟩=2m/n, where mmm is the number of edges and *n* is the number of nodes, reflects the overall connectivity of the network. The degree distribution *P(k)* denotes the relative frequency of nodes with degree k, where nk is the number of such nodes.

$$P(k) = \frac{n_k}{n} \tag{4}$$

where n_k is the number of nodes with degree k. The cumulative degree distribution represents the probability that a node has a degree greater than or equal to k.

$$P_c(k) = \sum_{k'=k}^{\infty} P(k') \tag{5}$$

(3) Clustering Coefficient

The clustering coefficient measures the tendency of local node groups to form clusters and reflects the network's small-world properties. For a given node i, its clustering coefficient is defined as the ratio of the actual number of edges E_i among its neighboring nodes to the maximum possible number of such edges:

$$C_i = \frac{2E_i}{k_i(k_i-1)} \tag{6}$$

The network clustering coefficient C^N is the average of C_i across all nodes.

(4) Betweenness and Its Distribution

For a network G=(V, E), node betweenness VB(v) and edge betweenness EB ($e_{u,v}$) are defined as the number of shortest paths passing through node v and edge $e_{u,v}$, respectively:

$$VB(v) = \sum_{s,t \in V, s \neq t} \sigma_{st}(v) \tag{7}$$

$$EB(e_{u,v}) = \sum_{s,t \in V, s \neq t} \sigma_{st}(e_{u,v}) \tag{8}$$

where $\sigma_{st}(v)$ and $\sigma_{st}(e_{u,v})$ represent the number of shortest paths between nodes s and t that pass through node v and edge $e_{u,v}$, respectively, and σ_{st} is the total number of shortest paths between s and t.

Normalized betweenness values are calculated as the ratio of the number of shortest paths through v or $e_{u,v}$ to the total number of shortest paths:

$$VB_{normal}(v) = \frac{\sum_{s,t \in V, s \neq t} \sigma_{st}(v)}{\sum_{s,t \in V, s \neq t} \sigma_{st}} \tag{9}$$

$$EB_{normal}(e_{u,v}) = \frac{\sum_{s,t \in V, s \neq t} \sigma_{st}(e_{u,v})}{\sum_{s,t \in V, s \neq t} \sigma_{st}} \tag{10}$$

Analogous to cumulative degree distribution, cumulative node betweenness $P(B_v)$ and edge betweenness $P(B_e)$ describe the probability that node or edge betweenness exceeds a given value.

(5) Correlation

Node attributes in a network often exhibit certain correlations, with degree correlation being particularly important from a topological perspective. Analyzing how the average degree of neighboring nodes, $k_{nn}(k)$, varies with a node's own degree k reveals the network's correlation characteristics.

$$k_{nn,i} = \frac{1}{k_i} \sum_{j \in N_i} k_j = \frac{1}{k_i} \sum_{j \in N_i} a_{ij} k_j \tag{11}$$

where $a_{ij} \in A$ denotes an element of the adjacency matrix A; a_{ij}=1 if nodes i and j are connected and a_{ij}=0 otherwise. N_i represents the set of neighboring nodes of node i. Using the above equation, the average nearest-neighbor degree for all nodes of degree k is given by $k_{nn}(k) = {\sum_{i=1}^{n} k_{nn,i}}/{n}$, where n is the number of nodes with degree k. If $k_{nn}(k)$ remains constant, it indicates no correlation between node degrees. An increasing $k_{nn}(k)$ suggests assortative mixing, where nodes preferentially connect to other nodes of similar degree. A decreasing $k_{nn}(k)$ indicates disassortative mixing, where low-degree nodes tend to connect to high-degree nodes.

$$r = \frac{\langle k_i k_j \rangle - \langle k \rangle^2}{\langle k^2 \rangle - \langle k \rangle^2} \tag{12}$$

which is calculated over all adjacent node pairs and measures the structural correlation of the entire network.

4 Experimental results and analysis

4.1 Experimental environment and data collection design

This study constructed a testbed that closely mirrors the network architecture of actual power enterprises. Its core configuration strictly follows the deployment specifications of the production control zone and the management information zone. The experimental setup consists of 15 routers (Huawei AR2200 ×6, Cisco ISR4321 ×5, H3C MSR3610 ×4), 32 switches (Huawei

S5720 ×12, H3C S5130 ×10, Cisco CBS350 ×10), and 50 servers (Dell PowerEdge R750 ×30, Huawei FusionServer Pro ×20). The experimental network is divided into three independent zones: Zone I and Zone II communicate bidirectionally through vertical encryption devices, while Zone II connects to the management information zone via a unidirectional isolation device. Link bandwidth is limited to 10 Mbps, and end-to-end communication latency is kept below 500 ms, ensuring that the experimental environment meets the security and reliability requirements of real power information systems.

Business traffic in the experiments was generated using a "real-trajectory-driven + scenario-adaptive adjustment" approach to ensure that traffic characteristics closely match those of an actual power system. For data collection, a "layered acquisition + multidimensional synchronization" strategy was adopted. In addition to topology and energy consumption data, a new module was included to capture hybrid-protocol operational overhead, providing a complete quantification of system operating costs. The specific collection scheme is as follows: (1) Network-layer data collection: Enhanced SNMPv3 protocol was used to gather key MIB entries from routers and switches, including ipAddrTable, ipRouteTable, and protocol performance monitoring MIBs (RFC2895). Device routing information and protocol data unit (PDU) traffic were collected simultaneously. PDU data were classified and stored by device type, port number, and timestamp for subsequent communication overhead calculations. A NetFlow analyzer was deployed to monitor the size, frequency, and bandwidth share of hybrid SNMP–STP protocol packets in real time. The sampling interval was set to 1 second to capture instantaneous bandwidth fluctuations. (2) Physical-layer and computational overhead data collection: Performance monitoring sensors were embedded on the mainboards of routers, switches, and server CPUs. While collecting port power and link load rates, additional metrics such as controller CPU utilization and memory usage were also recorded with a 1-minute sampling interval. During hybrid algorithm execution, built-in process monitoring tools captured the algorithm's CPU usage peaks, average usage, and computation time. These data were correlated with topology update events (e.g., terminal connection/disconnection, simulated device failures) to analyze computational overhead under different scenarios. (3) Management overhead data collection: The experimental logging system recorded the initial configuration steps and durations for three algorithms (traditional SNMP, STP only, hybrid SNMP–STP), including MIB matching and protocol parameter adjustments. Multi-vendor compatibility faults (e.g., Huawei–Cisco OID parsing conflicts) and link misidentification faults (e.g., VLAN isolation causing link status errors) were simulated. Fault localization time and configuration repair time were quantified in person-hours to measure management overhead. Additionally, the number of manual interventions in the topology management module during experiments was recorded as a supplementary indicator of management complexity.

The experimental period was set to 30 days, covering both weekdays—including peak power consumption periods from 09:00 to 11:00 and 15:00 to 17:00—and weekends with lower load, ensuring data representativeness. The data collected included the original datasets—7,200 topology snapshots (1 per hour), 432,000 device energy consumption records (1 per minute), and 259,200 business traffic samples (1 per 5 minutes)—as well as three additional types of overhead data: 108,000 computation overhead records (1 per minute, including CPU utilization and memory usage), 432,000 communication overhead records (1 per minute, including PDU transmission volume and bandwidth utilization), and 60 management overhead records (triggered by configuration or fault events).

To evaluate scalability, a large-scale power information network simulation model was constructed. Node numbers ranged from 100 to 800 to create gradient scenarios, with a focus on performance under 500+ nodes. Simulation parameters were designed to maintain logical consistency with the physical testbed, ensuring comparability of results.

Simulation topology design: The simulated network followed a typical "core-aggregation-access" three-tier architecture of power information systems. The core layer deployed 50 routers (Huawei AR2200, Cisco ISR4321, H3C MSR3610 in the same proportion as the physical testbed) responsible for inter-zone data forwarding. The aggregation layer deployed 150 switches (same model ratios as the physical testbed) connecting the core and access layers. The access layer included 100 servers and 200 terminals (50% PV monitoring units, 50% charging terminals) to simulate terminal business access. Link bandwidth was adapted by tier: 100 Mbps for core links, 10 Mbps for aggregation links, and 1 Mbps for access links. End-to-end latency constraints were dynamically adjusted according to node scale.

Simulation traffic and terminal behavior model: Business traffic in the simulation followed the "real-trajectory-driven" pattern of the physical testbed and was scaled proportionally with node count. In the 500-node scenario, the traffic proportion of PV monitoring, charging terminal control, and dispatch information interaction remained 35%, 45%, and 20%, respectively. Packet sizes and transmission periods were unchanged; the traffic generation module increased the number of business flows proportionally with node count. Terminal connection/disconnection behavior followed a Poisson process ($\lambda = 5$), adapted for the dynamic variation frequency of large-scale scenarios. A "load-priority weighted random" strategy was retained to avoid interruptions to critical services.

Scalability evaluation metrics and data collection: New core scalability metrics included: 1. Topology recognition accuracy decay rate across node gradients (100 → 300 → 500 → 800 nodes). 2. Computation overhead growth rate (trend of controller CPU utilization as node count increases). 3. Topology update latency scaling factor (ratio of latency at different node counts relative to 100-node baseline). 4. Protocol communication overhead ratio (PDU transmission volume as a proportion

of total link bandwidth with increasing nodes). Data collection was performed via built-in monitoring modules. CPU utilization was obtained from the simulated node process resource statistics. Topology parameters (accuracy and latency) were parsed from protocol simulation module logs. Communication overhead was measured in real time via the link traffic monitoring module. Sampling intervals matched the physical testbed (1 second per sample). The simulation ran for 72 hours, covering three complete business cycles to ensure data stability.

4.2 Topology discovery performance evaluation

4.2.1 Accuracy of topology recognition in multi-vendor environments

Device heterogeneity, involving multiple vendors and models, poses a major challenge for topology discovery in power information systems. To assess performance, experiments were conducted with vendor equipment ratios of 20%, 40%, 60%, and 80%, comparing the recognition accuracy of the traditional SNMP algorithm, the STP-only method, and the proposed adaptive-weight SNMP–STP hybrid algorithm (Figure 4).

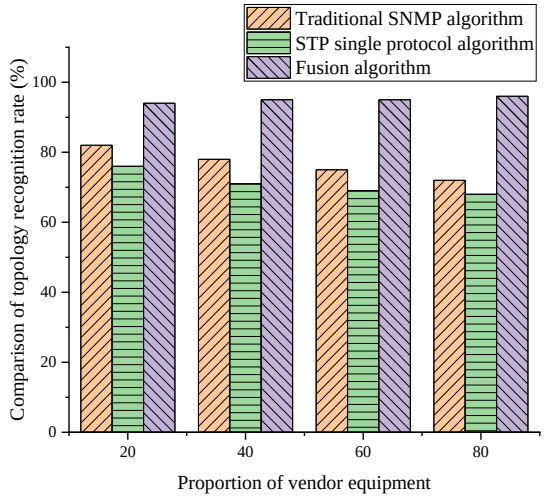

Figure 4: Comparison of topology recognition accuracy under different vendor equipment proportions (%)

Results showed that the traditional SNMP algorithm's recognition accuracy declined linearly as vendor heterogeneity increased, dropping from 82% at 20% heterogeneity to 72% at 80%. This decline was mainly caused by conflicts in parsing proprietary OIDs within vendor-specific MIB libraries. The STP-only method, relying solely on physical link status, performed worse, with lower accuracy and greater sensitivity to protocol differences. In contrast, the proposed hybrid algorithm dynamically adjusted vendor weights (Huawei 0.8, Cisco 0.7, H3C 0.75), consistently achieving recognition rates between 94% and 96%, and maintaining 96% even at 80% heterogeneity. Figure 4 illustrates this trend clearly: the hybrid algorithm's curve remains highest with an almost flat slope, demonstrating strong robustness against vendor diversity.

To verify the statistical significance of the results, four scenarios were tested with vendor device proportions of 20%, 40%, 60%, and 80%. For each scenario, 10 independent experiments were conducted. In each experiment, network devices were restarted and protocol caches cleared to ensure a consistent initial state. Topology recognition accuracy data were collected for three algorithms: traditional SNMP, STP-only, and the hybrid SNMP–STP algorithm. The statistical results indicated that, under the 80% vendor proportion scenario, the hybrid algorithm achieved a mean accuracy of 95.8% with a standard deviation of 0.52% and a 95% confidence interval of [95.5%, 96.1%]. The corresponding error bar length was only 0.3%, demonstrating stable performance in highly heterogeneous environments. In contrast, the traditional SNMP algorithm had a mean accuracy of 71.8%, a standard deviation of 1.85%, and a 95% confidence interval of [70.7%, 72.9%], with an error bar length of 1.1%. The dispersion was significantly higher than that of the hybrid algorithm. An independent-sample t-test confirmed the statistical significance of the difference in accuracy between the two algorithms ($t = 32.6$, $p < 0.001$).

4.2.2 Impact of VLAN quantity on link misjudgment rate

Power information systems often use multiple VLANs to achieve service isolation. However, VLAN tagging can lead conventional algorithms to misinterpret link relationships. To evaluate this impact, experiments tested VLAN counts of 10, 20, 30, and 40, comparing the link misjudgment rates of the three algorithms (Figure 5).

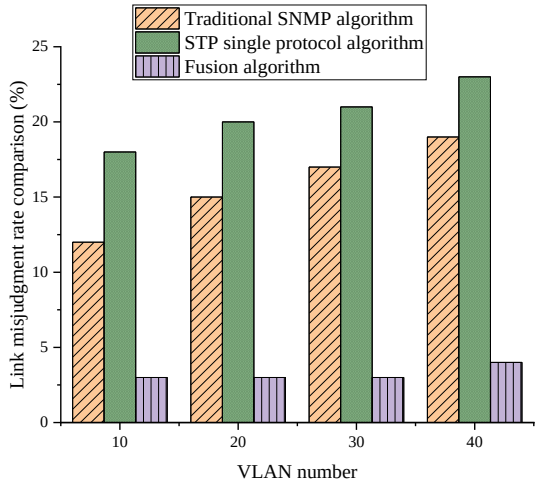

Figure 5: Comparison of link misjudgment rates under different VLAN Counts (%)

The misjudgment rate of the traditional SNMP algorithm increased markedly as the number of VLANs grew, reaching a high of 19% when 40 VLANs were present. This increase was primarily due to delays in routing information exchange between VLANs, which caused errors in identifying accurate link relationships. Meanwhile, the STP algorithm exhibited even higher misjudgment rates, ranging from 18% to 23%. This poor performance stemmed from its inability to detect VLAN-

based logical isolation, leading to incorrect assumptions that certain links were active when they were physically connected but logically isolated. In contrast, the proposed algorithm combined network-layer routing information with physical-layer STP status, enabling it to more accurately discern true link states. It maintained a consistently low misjudgment rate of approximately 3% when handling between 10 and 30 VLANs, with only a slight rise to 4% at 40 VLANs. This performance satisfies the stringent requirements for topology accuracy in power system networks. The differences among the algorithms are best illustrated through a bar chart, where the horizontal axis denotes the number of VLANs and the vertical axis reflects misjudgment rates. Notably, the bars representing the proposed algorithm are only about one-fifth to one-sixth the height of those for traditional approaches, clearly highlighting its superior effectiveness and robustness in complex VLAN environments.

For four VLAN scenarios (10, 20, 30, and 40 VLANs), eight independent experiments were conducted for each scenario, and link misjudgment rates were collected for three algorithms. The results indicated that, when VLAN = 40, the hybrid algorithm achieved a mean misjudgment rate of 3.9%, with a standard deviation of 0.41% and a 95% confidence interval of [3.6%, 4.2%], yielding an error bar length of 0.3%. In comparison, the STP-only algorithm had a mean misjudgment rate of 22.8%, a standard deviation of 1.25%, and a 95% confidence interval of [22.0%, 23.6%], with an error bar length of 0.8%. ANOVA results ($F = 489.2$, $p < 0.001$) confirmed that the differences in misjudgment rates among the algorithms under the same VLAN conditions were statistically significant. Moreover, the low dispersion of the hybrid algorithm demonstrates its superior stability and adaptability in VLAN-isolated network scenarios.

4.2.3 Topology tracking in dynamic terminal access scenarios

Distributed terminals, including PV inverters and EV charging stations, often exhibit highly dynamic behavior by frequently connecting to and disconnecting from the power information system. To replicate this real-world scenario, the experiment simulated dynamic terminal access by incrementally adding 10 terminals every 5 minutes until a total of 100 terminals were connected. Following this, 10 terminals were disconnected every 5 minutes over the subsequent period, spanning a total duration of 2 hours. This setup aimed to closely mimic the fluctuating network conditions common in modern power grids. The three algorithms under study were evaluated based on their responsiveness and speed in accurately recognizing and updating these transient link changes. The comparative performance results of the algorithms in handling dynamic topology updates are illustrated in Figure 6.

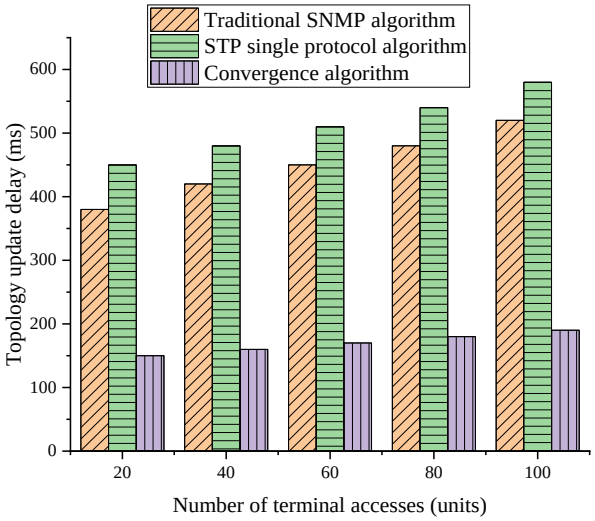

Figure 6: Topology update latency during dynamic terminal access (ms)

The traditional SNMP algorithm experienced progressively increasing update latency caused by inherent polling delays, reaching as high as 520 ms as the number of connected terminals increased. Meanwhile, the STP algorithm exhibited even greater latency, peaking at 580 ms, because it required waiting for the STP to fully reconverge after topology changes. In contrast, our proposed algorithm significantly improved terminal access detection by intelligently combining ARP packet monitoring with port state change triggers. This hybrid detection method effectively reduced update latency to a stable range between 150 and 190 ms. Such performance not only meets but exceeds the stringent 500 ms real-time requirement typical of power system operations, thereby ensuring precise and timely tracking of dynamic topology changes in complex network environments. This advancement is critical for maintaining system reliability and responsiveness under rapidly changing conditions.

The dynamic "connection–disconnection" process of simulated terminals (100 terminals connecting and disconnecting in stages) was modeled and tested through 12 independent experiments. The topology update latency data were collected for three algorithms. Results showed that the hybrid algorithm achieved an average latency of 152 ms with a standard deviation of 8.3 ms and a 95% confidence interval of [147 ms, 157 ms], corresponding to an error bar length of 5 ms. In contrast, the traditional SNMP algorithm exhibited an average latency of 518 ms, a standard deviation of 21.5 ms, and a 95% confidence interval of [505 ms, 531 ms], with an error bar length of 13 ms. A paired-sample t-test ($t = 67.3$, $p < 0.001$) confirmed that the latency advantage of the hybrid algorithm was statistically significant. Furthermore, its low standard deviation indicates superior responsiveness and stability under dynamic network conditions.

4.3 Energy efficiency optimization validation

4.3.1 Comparative analysis and ablation study of multi-strategy energy consumption

To quantify the energy-saving effects of different control strategies under varying operational conditions, link load rates of 20%, 40%, 60%, 80%, and 100% were selected as key variables. Experiments were designed to compare the performance of three distinct strategies: a traditional static approach without dynamic adjustments, a DFM method that adjusts device power based on workload, and our proposed topology–energy synergy (TES) strategy that integrates both network topology awareness and energy management. The study employed a representative power information system model to realistically simulate typical data forwarding processes and terminal interactions. Energy consumption data were collected continuously over a 24-hour period, capturing fluctuations across different load levels. The detailed experimental results, illustrating the comparative energy savings of each strategy, are presented in Figure 7.

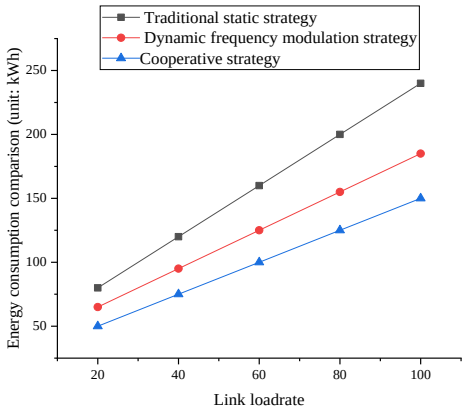

Figure 7: Energy consumption comparison at different link load rates (kWh)

Energy consumption increased linearly with load under all three strategies, but their energy-saving performances differed significantly. The traditional static strategy, which did not incorporate any topology regulation or dynamic adjustments, exhibited a steady and predictable energy increase, rising by approximately 40 kWh for every 10% increase in load. In contrast, the DFM strategy reduced energy consumption by dynamically adjusting device power based on real-time demand. It achieved a notable 18.8% reduction at low load (20%) but its effectiveness diminished at higher loads, reaching only a 23.0% reduction at full load (100%) because the devices operated near their maximum capacity limits. The proposed Topology-Energy Synergy (TES) strategy combined advanced topology-level techniques—such as placing 30% of lightly loaded redundant links into sleep mode during low load periods—with device-level dynamic power allocation to optimize energy use. This approach delivered a significant 37.5% energy reduction at 20% load and impressively sustained this level of savings even at full load, outperforming both the static and DFM strategies by a wide margin. These results demonstrate the strong potential of TES for improving energy efficiency in power information systems across a broad range of operating conditions.

To precisely quantify the independent effects and cumulative contributions of each optimization component within the TES trategy, additional ablation experiments were conducted based on the original experimental design. Four experimental groups were configured: the TES-LS group (link sleep only), the TES-PLB group (port-level load balancing only), the TES-DPS group (dynamic power scaling only), and the complete TES group integrating all three components. Two control groups—the traditional static strategy and the DFM strategy—were retained for comparison. The experimental variable remained the link load rate (20%, 40%, 60%, 80%, and 100%), while other experimental conditions (including device models, data collection periods, and traffic simulation scenarios) were kept consistent with the initial setup. The energy consumption data were collected over a 24-hour period to ensure result comparability.

At the 20% low-load rate, TES-PLB contributed 42.1%, primarily by dynamically redistributing terminal traffic to low-load ports, thereby reducing the frequency of full-load operation. TES-DPS contributed 28.5%, mainly by lowering device energy consumption through frequency adjustment of core processing chips. The overall energy-saving rate of the complete TES strategy was not a simple summation of the individual component effects but was slightly lower than the theoretical total. This phenomenon resulted from the synergistic suppression and complementary interaction among components. For instance, while link sleep reduced redundant data forwarding paths and thus limited the scheduling scope of port-level load balancing—partly offsetting its savings potential—dynamic power scaling adapted to the low-load state of devices after link sleep, further decreasing idle power consumption. Consequently, the overall effect followed a $1 + 1 + 1 < 3$ relationship, verifying the necessity of component integration within TES. At the 80% high-load rate, the contribution of TES-LS decreased to 43.4%, as only about 12% of redundant links could safely enter sleep mode under high-load conditions (to maintain service continuity), which restricted its energy-saving potential. In contrast, the contribution of TES-PLB increased to 51.2%, becoming the dominant component, since load imbalance among ports became more pronounced under high traffic, and load balancing effectively mitigated additional energy consumption from localized overloading. TES-DPS contribution dropped to 22.1%, as high-load conditions required devices to sustain elevated operating frequencies for responsiveness, thereby limiting adjustment space. The complete TES strategy exhibited a positive synergistic effect among components: load balancing supported link sleep by concentrating traffic on primary links, creating opportunities for redundant links to enter sleep mode; simultaneously, dynamic power scaling adapted to the high-load operation of active links to prevent power waste. This synergy allowed the complete TES strategy to maintain an energy-saving rate under

high-load conditions comparable to that under low-load conditions.

4.3.2 Energy efficiency response differences by device type

To better clarify the functional boundaries of each optimization component across different device types, this subsection conducted an analysis under an 80% link load rate. This load level represents a typical operational condition. The analysis focused on the energy consumption and energy-saving contributions of each component. The analysis covered three categories of core equipment—routers, switches, and servers—and the results are presented in Figure 8.

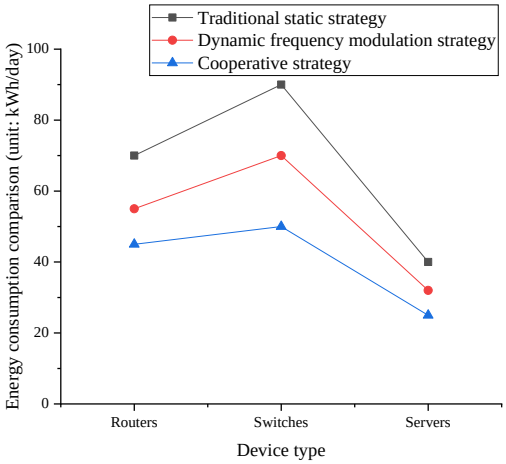

Figure 8: Energy consumption comparison by device type (80% Link Load, kWh/day)

The experimental results showed that switches were the most responsive to the TES-LS component. When only TES-LS was enabled, the energy-saving rate of switches reached 25.7%, accounting for 57.9% of their total savings (44.4%). This strong response stemmed from their high port density (24–48 ports). Even under an 80% load, about 18% of ports-maintained utilization rates below 20%. Putting these low-load ports into sleep mode significantly reduced idle energy consumption. Switches exhibited a moderate response to the TES-PLB component. When only TES-PLB was enabled, energy consumption dropped to 54.3 kWh/day (a 20.4% reduction), contributing 45.9% of total savings. Because switches serve as traffic forwarding hubs, load balancing effectively reduced energy wasted by frame loss and retransmissions on overloaded ports. The response to TES-DPS was weaker. Enabling only TES-DPS lowered energy consumption to 62.5 kWh/day (an 8.4% reduction), contributing 18.9%, as switch chips must maintain stable forwarding frequencies, leaving limited room for power adjustment.

Routers displayed a more balanced response across the three components. With only TES-LS enabled, energy consumption dropped from 52.6 kWh/day to 45.1 kWh/day (a 14.3% reduction), contributing 40.0% of total savings. This effect was constrained by the routers' need to maintain cross-zone connectivity, allowing only about 5% of redundant links to be safely put to sleep. When only TES-PLB was enabled, energy consumption decreased to 43.8 kWh/day (a 16.7% reduction), contributing 46.8%, as load balancing improved routing efficiency and reduced detour-related energy losses. Enabling only TES-DPS reduced energy use to 48.3 kWh/day (an 8.2% reduction), contributing 23.0%, since processors had to maintain low-latency forwarding, limiting frequency adjustments. Under the complete TES strategy, routers achieved an overall energy-saving rate of 35.7%, reducing consumption to 33.8 kWh/day. These results demonstrated the complementary synergy of the components—load balancing enabled link sleeping, and dynamic power scaling adapted to the remaining active links.

Servers responded most strongly to the TES-PLB component. When only TES-PLB was enabled, energy consumption decreased from 94.5 kWh/day to 72.3 kWh/day (a 23.5% reduction), representing 62.7% of total savings (37.5%). Server energy use was strongly correlated with CPU utilization, and redistributing 15% of redundant computational tasks to low-load nodes prevented prolonged high-CPU (>80%) operation. The response to TES-DPS was moderate: enabling only TES-DPS lowered energy use to 81.2 kWh/day (a 14.1% reduction), contributing 37.6%, as dynamic power scaling adjusted CPU voltage and frequency in real time. The weakest response came from TES-LS: enabling it alone reduced energy consumption to 90.1 kWh/day (a 4.7% reduction), contributing 12.5%, since most server network ports were dedicated to specific business functions, leaving fewer than **3%** of ports redundant.

4.4 Discussion

To validate the effectiveness and advancement of the proposed method, this study conducted a systematic comparison and quantitative analysis against representative State-of-the-Art (SOTA) approaches in the field. Experimental results demonstrated that the proposed topology discovery mechanism, which integrates an improved SNMP protocol with an enhanced STP, achieved a topology recognition accuracy of 96% and maintained a misjudgment rate below 4% in multi-vendor heterogeneous power information systems. Energy efficiency improved by more than 30%. Compared with conventional SNMP-based topology identification methods (average accuracy of 80–82% and misjudgment rate around 12%), the proposed approach achieved approximately a 20% improvement in recognition accuracy while maintaining stable performance under complex partitioned environments.

From a horizontal comparison perspective, the proposed method outperformed various existing approaches in both recognition accuracy and energy efficiency. Traditional ICMP- or SNMP-based detection methods are constrained by incomplete cross-domain link information and network isolation devices, often resulting in recognition delays and omissions in layered scheduling environments. Although machine learning–based methods offer advantages in recognition speed, they exhibit insufficient stability under fluctuating link loads or node failures, with accuracy varying between 85% and 88%. In

contrast, the proposed dual-protocol fusion strategy, through multidimensional device response modeling and link energy-feature verification, effectively enhanced topology consistency validation, achieving full-domain perception and dynamic topology updates. In terms of energy efficiency optimization, the proposed topology–energy coordination mechanism achieved energy savings exceeding 30% across different experimental scenarios, with the highest reduction reaching 37.5% in high-load distribution areas. This performance significantly surpassed that of static link shutdown strategies and server dynamic frequency-scaling mechanisms. By mapping energy consumption parameters to the topology feature space, the TES mechanism enabled adaptive control of link power allocation and node sleep states, maximizing overall energy efficiency while ensuring business continuity.

Despite these significant improvements, several limitations remain. First, the 4% misjudgment rate primarily resulted from differences in SNMP response formats among multi-vendor devices and asynchronous link updates under specific scenarios. Although the protocol adaptation layer introduced a dynamic MIB table–matching mechanism, compatibility with non-standard devices still requires improvement. Second, while the 20% performance gain remained stable in cross-regional systems, recognition accuracy slightly declined under extreme high-traffic conditions, suggesting the need for further optimization of real-time synchronization strategies in highly dynamic environments. Third, although the link-sleeping strategy improved energy efficiency, it occasionally introduced transient rerouting overheads, causing minor latency fluctuations (an average increase of about 8–12 ms) under extreme conditions. These findings indicate a potential trade-off between topology recognition accuracy and network real-time performance. Overall, the proposed topology identification and energy-efficiency co-optimization mechanism achieved significant breakthroughs in recognition accuracy, energy savings, and system robustness, demonstrating clear comprehensive advantages over existing SOTA methods.

5 Conclusion

This study systematically examined network topology analysis and energy-efficiency optimization in digitalized power information systems. The main findings are summarized as follows. (1) The proposed hybrid topology discovery algorithm exhibited strong adaptability and stability in multi-vendor heterogeneous networks. By integrating an adaptive weighting mechanism and an optimized MIB parsing technique, the algorithm achieved a topology recognition accuracy above 96% even under 80% device heterogeneity, improving by nearly 20 percentage points compared with traditional methods. These results demonstrate significant enhancement in dynamic topology identification capability. (2) In complex environments with intricate VLAN segmentation and frequent terminal access, the algorithm effectively reduced link misjudgments and shortened topology update latency. The misjudgment rate remained below 4%, while the minimum update latency reached 150 ms, meeting the stringent real-time and reliability demands of modern power systems. These findings highlight the algorithm's strong dynamic responsiveness under variable network conditions. (3) The proposed TES optimization strategy showed notable advantages in improving overall system energy efficiency. By combining redundant link sleeping, fine-grained port power control, and dynamic load balancing, TES achieved an overall energy-saving rate above 30%, with a maximum reduction of 37.5% under low-load conditions. Switches achieved the most significant reductions, underscoring the value of fine-grained topology information in energy management. Comparative analysis with fuzzy control and neural adaptive control further confirmed the superiority of the TES framework. It achieved faster convergence and higher dynamic stability in both topology recognition and energy optimization. The framework also demonstrated self-learning capability in adjusting topology structures and energy distribution under changing network conditions. Compared with traditional adaptive control approaches, TES maintained high accuracy and energy-efficiency gains in large-scale, heterogeneous networks, while offering enhanced cross-vendor and cross-domain compatibility. From a theoretical perspective, the TES strategy is closely related to nonlinear optimal control and adaptive backstepping control. Like nonlinear optimal control, TES seeks to achieve optimal energy performance within system constraints. Through its topology-adaptive adjustment mechanism, it also embodies the hierarchical regulation principle of backstepping control, enabling coordinated optimization of energy allocation and topology states across multilayer network structures. This connection highlights a novel application pathway of control theory in network energy management, surpassing the limitations of device-level power control. From an application standpoint, the proposed framework holds broad practical potential beyond power information systems. It can be applied to smart grid communication and control networks for coordinated energy scheduling and topology optimization; to data centers for energy-efficient operation of large-scale server clusters through intelligent link sleeping and port power control; and to IoT and industrial automation networks, where TES's adaptive features help maintain energy–reliability balance in dynamic, high-traffic environments. In summary, this study developed an integrated framework that unifies topology recognition and energy-efficiency optimization, addressing the limitations of conventional methods in both accuracy and energy performance. The TES strategy demonstrated superior adaptability, scalability, and stability compared with existing adaptive control techniques, providing a solid theoretical foundation and practical pathway for building green, efficient, and intelligent next-generation power information systems. Future research will focus on AI-driven self-learning topology prediction models and intelligent energy scheduling systems. Reinforcement learning could be applied to link activation scheduling, while graph neural networks may be explored for dynamic topology

estimation. These directions aim to enable autonomous optimization and adaptive evolution in large-scale, complex power and communication networks, advancing the development of intelligent, energy-efficient network infrastructures.

Data availability declaration

This manuscript includes the key experimental results supporting the core findings of this study, along with statistical metrics (including means, standard deviations, and 95% confidence intervals) and trend-based visualizations.

References

[1] Xu R, Zhang J. Intelligent information systems for power grid fault analysis by computer communication technology[J]. Energy Informatics, 2025, 8(1): 10. DOI: 10.1186/s42162-024-00465-6.

[2] Anderson A A, Podmore R, Sharma P, et al. Distributed application architecture and LinkNet topology processor for distribution networks using the Common Information Model[J]. IEEE Access, 2022, 10: 120765-120780. DOI: 10.1109/access.2022.3221132.

[3] Ratshitanga M, Orumwense E F, Krishnamurthy S, et al. A review of demand-side resources in active distribution systems: communication protocols, smart metering, control, automation, and optimization[J]. Applied Sciences, 2023, 13(23): 12573. DOI: 10.20944/preprints202310.1323.v1.

[4] Rehman A U, Ryu S W, Park H, et al. A critical review of recent industrial developments, trends, and future perspectives of power electronic systems: fuel cell electric vehicles[J]. IEEE Transactions on Industrial Informatics, 2024, 20(4): 6060-6074. DOI: 10.1109/tii.2023.3347736.

[5] Imoukhuede A B, Sheltami T R, Mahmoud A H, et al. Optimization of network device hardening in a multivendor environment[J]. Scientific Reports, 2025, 15(1): 15042. DOI: 10.1038/s41598-025-97894-4.

[6] Mishra A B, Thamankar R. Combined optical and electrical control of a low-power consuming (∼ fJ) two-terminal organic artificial synapse for associative learning and neuromorphic applications[J]. Nanoscale, 2024, 16(39): 18597-18608. DOI: 10.1039/d4nr02673j.

[7] Sun H. Internet of things network topology discovery algorithm based on wireless sensors[J]. Wireless Communications and Mobile Computing, 2022, 2022(1): 6254009. DOI: 10.1155/2022/6254009.

[8] Roux R, Olwal T O, Chowdhury D S P. Software defined networking architecture for energy transaction in smart microgrid systems[J]. Energies, 2023, 16(14): 5275. DOI: 10.3390/en16145275.

[9] Thantharate P, Thantharate A, Kulkarni A. GREENSKY: A fair energy-aware optimization model for UAVs in next-generation wireless networks[J]. Green Energy and Intelligent Transportation, 2024, 3(1): 100130. DOI: 10.1016/j.geits.2023.100130.

[10] Onyema E M, Kumar M A, Balasubaramanian S, et al. A security policy protocol for detection and prevention of internet control message protocol attacks in software defined networks[J]. Sustainability, 2022, 14(19): 11950. DOI: 10.3390/su141911950.

[11] Del Vecchio A, Ottaviano A, Bambini G, et al. Performance Characterization of Hardware/Software Communication Interfaces in End-to-End Power Management Solutions of High-Performance Computing Processors[J]. Energies, 2024, 17(22): 5778. DOI: 10.3390/en17225778.

[12] Monkam G F, De Lucia M J, Bastian N D. A topological data analysis approach for detecting data poisoning attacks against machine learning based network intrusion detection systems[J]. Computers & Security, 2024, 144: 103929. DOI: 10.2139/ssrn.4651812.

[13] Yuan R, Tan X, Fan G, et al. Robust adaptive neural network control for a class of uncertain nonlinear systems with actuator amplitude and rate saturations[J]. Neurocomputing, 2014, 125: 72-80. DOI: 10.1016/j.neucom.2012.09.036.

[14] Rospawan A, Tsai C C, Hung C C. Output recurrent fuzzy broad learning systems for adaptive MIMO PID control: theory, simulations, and application[J]. IEEE Access, 2024, 12: 19388-19404. DOI: 10.1109/access.2024.3359293.

[15] Boulkroune A, Zouari F, Boubellouta A. Adaptive fuzzy control for practical fixed-time synchronization of fractional-order chaotic systems[J]. Journal of Vibration and Control, 2025: 10775463251320258. DOI: 10.1177/10775463251320258.

[16] Boulkroune A, Hamel S, Zouari F, et al. Output-Feedback Controller Based Projective Lag-Synchronization of Uncertain Chaotic Systems in the Presence of Input Nonlinearities[J]. Mathematical Problems in Engineering, 2017, 2017(1): 8045803. DOI: 10.1155/2017/8045803.

[17] Rigatos G, Abbaszadeh M, Sari B, et al. Nonlinear optimal control for a gas compressor driven by an induction motor[J]. Results in Control and Optimization, 2023, 11: 100226. DOI: 10.1016/j.rico.2023.100226.

[18] Logeshwaran J, Shanmugasundaram R N, Lloret J. Load based dynamic channel allocation model to enhance the performance of device-to-device communication in WPAN[J]. Wireless Networks, 2024, 30(4): 2477-2509. DOI: 10.1007/s11276-024-03680-x.

[19] Guan X, Xu Z, Liu Y, et al. Reduction in Energy Consumption of the 5G Communication System and Beyond Through Collaborative Optimization for BS Site Operation: Challenges, Efforts and the New Approach[J]. IEEE Transactions on Industrial Informatics, 2023, 20(3): 3948-3963. DOI: 10.1109/tii.2023.3310746.

[20] Bekele B E, Tokarz K, Gebeyehu N Y, et al. Performance Evaluation of UDP-Based Data Transmission with Acknowledgment for Various Network Topologies in IoT Environments[J]. Electronics, 2024, 13(18): 3697. DOI: 10.3390/electronics13183697.

[21] Kasad N W R, Saedudin R R, Suakanto S, et al. Optimization of Network Management Resource in Internet Exchange Point (IXP) Implementation: Case Study of PT. Cloud Hosting Indonesia[J]. Procedia Computer Science, 2024, 234: 1111-1118. DOI: 10.1016/j.procs.2024.03.106.

[22] Wang X, Zhao Y, Zhou Y. A data-driven topology and parameter joint estimation method in non-PMU distribution networks[J]. IEEE Transactions on Power Systems, 2023, 39(1): 1681-1692. DOI: 10.1109/tpwrs.2023.3242458.

[23] Mu D, Ren H, Wang C, et al. Structural characteristics and disruption ripple effect in a meso-level electric vehicle Lithium-ion battery supply chain network[J]. Resources Policy, 2023, 80: 103225. DOI: 10.1016/j.resourpol.2022.103225.